Lithium-induced conversion reaction in wüstite Fe1-xO studied by 57Fe Mössbauer spectroscopy.

Laurent Aldon, Jean-Claude Jumas

Lithium-induced conversion reaction in wüstite $Fe_{1-x}O$ studied by ^{57}Fe Mössbauer spectroscopy

L. Aldon*, J.-C. Jumas

Institut Charles Gerhardt Montpellier
UMR 5253 CNRS-UM2-ENSCM-UM1
Université Montpellier 2
Agrégats, Interfaces et Matériaux pour l'Energie CC 1502, Place Eugène Bataillon 34095
Montpellier CEDEX 5 – France

*Corresponding author: laurent.aldon@um2.fr

ABSTRACT

$Fe_{1-x}O$ wüstite as negative electrode material for Li-ion batteries has been studied. The aim of this work is to get a better understanding of the insertion mechanism involved during reduction/oxidation processes. Electrochemical tests have been done in Swagelock^{TM} cells and shown a high specific capacity of 800 Ah/kg for the first discharge. X-ray diffraction and ^{57}Fe Mössbauer spectroscopy provide us valuable information on both local and long range order. Hence, Li reaction with wüstite induces formation of highly divided metallic iron (α-Fe and nano-Fe) and Li_2O with a small amount of Fe_2O_3 occurring in a diffusion layer at the surface of the primary particles. Based on the X-ray and Mössbauer spectroscopic analyses, a core-shell model is proposed in order to explain the irreversible capacity of about 1 Li observed at the first cycle. It involves cation diffusion induced by lithium acting as an 'electronic pressure'.

KEY WORDS: Wüstite, Mössbauer spectroscopy, Conversion reaction, Lithium, Electrochemical mechanism, Disproportionation, Irreversible capacity.

INTRODUCTION

Anodic materials having a discharge potential of 1V/Li are chosen among the metallic oxides [1,2]. Iron oxides are inexpensive and present low environmental impact for lithium battery applications [3,4]. Previous works have shown the interest of such iron oxides as electrochemically active material [5,6]. The mechanism is generally based upon the redox couple Fe^{3+}/Fe^{2+} working at approximately 0.5 V compared to lithium [7,8]. Wüstite is a non-stoichiometric compound with formulae $Fe_{1-x}O$, with $0.83 < x < 0.96$ [9]. It has the rocksalt structure with a cell parameter of 4.307 Å [10]. In the structure some Schottky defects occur because of the presence of two oxidation states Fe^{II} and Fe^{III}, occupying the octahedral sites of the structure. Fe^{II} is rather easy to oxidize to Fe^{III} and can explain the wide range of composition. In order to get a better understanding of electrochemical Li reaction mechanism into $Fe_{1-x}O$, the present work deals with ^{57}Fe Mössbauer spectroscopy, X-ray diffraction and electrochemical tests. Coupling these experimental techniques allows us to get deeper insight into the mechanism ruling lithium reaction processes in the $Fe_{1-x}O$ wüstite phase.

From X-ray diffraction, previous work has shown a correlation between amount of vacancies and cell parameters [11]. From ^{57}Fe Mössbauer spectroscopy the relative contribution of Fe^{II} and Fe^{III} to the spectrum can be determined [12, 13]. Hence comparison between the amount of vacancies from X-ray diffraction and Mössbauer spectroscopy can be done. This nuclear technique gives local information at the atomic scale and is very sensitive of the neighborhood in terms of charge of ions and vacancy effects [14, 15].

The electrochemical mechanism shows that a part of Li (~44 %) is involved in the reduction of FeO into metallic Fe^0 accompanied with small amount of nano-sized Fe_2O_3 and a last part of Li (~56 %) is consumed to form a SEI in the first discharge. This last part seems to

be responsible for the irreversible capacity in this conversion reaction. The reversible process is based on a reversible reaction: $Fe^{II}O + 2Li \leftrightarrow Fe^0 + Li_2O$.

EXPERIMENTAL

Synthesis conditions

Wüstite $Fe_{1-x}O$ has been prepared from powdered hematite α-Fe_2O_3 by specific heat treatment [9]. Hematite has been ground in an agate mortar and then the fine powder has been put into a porcelain crucible. The crucible is then placed in the quartz tube of the oven at 800 °C under H_2 atmosphere used as reducing agent [16]. Since $Fe_{1-x}O$ is metastable [17, 18] and decomposes below 570 °C to magnetite Fe_3O_4 and metallic Fe at ambient pressure and temperature, the crucible has been quenched outside by cooling with pulsed air.

X-ray diffraction

X-ray diffraction (XRD) patterns were collected on a conventional Philips θ-2θ diffractometer with Cu-K_α radiation (1.5418 Å) and a nickel filter in order to characterize the compounds before and after insertion of lithium. For electrochemically-inserted phase, the recording was made under vacuum in order to avoid undesirable reactions with air.

^{57}Fe Mössbauer spectroscopy

^{57}Fe Mössbauer spectra were recorded at room temperature (RT) using transmission geometry in the constant acceleration mode with a spectrometer based on electronic devices delivered by EG&G and WissEl. The absorbers contained 1-2 mg of ^{57}Fe per cm^2 were prepared inside the glove box, and sealed with parafilm to avoid contact with air. The velocity scale was calibrated using the 2 inner lines (*see below*) of the magnetic sextet of a high purity iron foil absorber as a standard, using ^{57}Co (Rh) as the source. The spectra were fitted using a Lorentzian approximation by least-squares method implemented in our GM5SIT program [19,

20]. The quality of the fit was controlled by the conventional χ^2 test. Isomer shift (IS) values are given relative to the centre of the α-Fe (10 μm foil) spectrum recorded at room temperature. The shape of a Mössbauer spectrum of a paramagnetic compound is generally determined by a doublet, characterized by the quadrupole splitting (QS) separating more or less the 2 Lorentzian lines and their mean position, the isomer shift (IS). The intensity of the absorption (A) is ruled by the number of sites (N) and the Lamb-Mössbauer factor (f) through A = N.f.

In the case of magnetic contribution, the spectrum is split into 6 Lorentzian lines with a relative intensity as 3:2:1:1:2:3. Mössbauer spectra of bulk α-Fe or Fe_2O_3 present such a magnetic sextet. The sextet of α-Fe used for velocity calibration is composed of two lines located at $IS_{1,6}$ = ±5.33 mm/s with relative intensities of 3, two other lines at $IS_{2,5}$ = ±3.02 mm/s with relative intensities of 2. The inner lines of the sextet have relative intensities of 1. Since we present in the following Mössbauer spectra recorded in a small velocity range [±2.4 mm/s] to favor details in the Fe^{III}/Fe^{II} velocity scale, we can only detect the two inner lines $IS_{3,4}$ = ±0.84 mm/s. For convenience, we choose to fit these two lines with an equivalent doublet with IS ~0 mm/s and QS ~1.68 mm/s. After convergence of the fitting procedure, we have to correct the total absorption of our sample. We have multiplied by 6 the relative contribution of this doublet to get the real contribution of metallic α-Fe in the mixture. The same procedure will be used with a magnetic contribution of Fe_2O_3. Then, all contributions are corrected to obtain the relative amount of the species.

Concerning the non-stoichiometric wüstite phase, $Fe_{1-x}O$ will be written taking into account the amount of vacancies, $\boldsymbol{x}$, as $Fe^{II}_{1-3x}Fe^{III}_{2x}\square_xO$. This quantity can be roughly estimated from the relative contributions A_{II} and A_{III} from the Mössbauer spectroscopic data by:

$$x = \frac{1}{3 + 2\, A_{II} / A_{III}}$$

It is thoroughly admitted in the Mössbauer community that vacancies or 'guest' ions can be detected in the vicinity of the probed ion or atom (^{57}Fe) from the quadrupole splitting distribution as shown by Womes *et al.* [21]. The presence of both Fe^{III} and vacancies in the vicinity of probed Fe^{II} may change the electric field gradient (EFG) and therefore the measured quadrupole splitting (QS). The quadrupole splitting reflects the ferrous quadrupole interaction in the paramagnetic state and is related to the elements of the diagonalized electric field gradient tensor that can be estimated for ionic compounds from point charge model calculations [22].

Assuming a random distribution [23, 24] of both vacancies and cations in the wüstite structure, the probability of a probed Fe^{II} to have n Fe^{III} ions, m vacancies at a concentration *x* and 12-m-n Fe^{II} located in the 12 neighboring sites of the first coordination shell of $Fe_{1-x}O$ is given by:

$$p_{n,m}(x) = \frac{12!}{n!m!(12-n-m)!} 2x^{n+m}(1-3x)^{12-n-m}$$

Since the solid solution domain is not very extended for $Fe_{1-x}O$ ($x < 0.1$), we think that the main contributions are due to electric charge as often observed for ionic compounds [25]. The most probable configurations will be grouped according to the values of *n* and *m*. For instance a Fe^{II} surrounded by n = 1 Fe^{III} and m = 0, 1 or 2 vacancies will give an intensity proportional to $P_1 = P_{1,0} + P_{1,1} + P_{1,2}$ if we neglect the cases where $m > 2$ since $x < 0.1$. Hence 3 main contributions $P_n = P_{n,0} + P_{n,1} + P_{n,2}$ (n = 0, 1 or 2) will be the most probable and expected configurations. In this case we believe that the measured quadrupole splitting will be n-dependant.

The intensity of the absorption of a given phase depends on its recoil-free factor f (named the Lamb-Mössbauer factor [26, 27]). The factor f depends on the Debye temperature,

θ_D, which decreases with decreasing particle size [28]. It is worth noticing that dispersed Fe nano-particles not bound to a rigid matrix show a large decrease in the apparent Debye temperature. Indeed the Debye temperature has been estimated to 388 ± 20 K for bulk α-Fe. This value decreases to 344 ± 16 K and 259 ± 18 K for particles of 2.5 nm and 1.5 nm in size, respectively [29]. For wüstite it has been estimated to θ_D = 417 K [30]. Knowing the Debye temperature of a given material, the Lamb-Mössbauer factor, which depends on the temperature and on the recoil energy (E_R = 1.956 meV for ^{57}Fe), can be estimated through:

$$\ln f_{LM}(T) = -\frac{6E_R.T}{k\vartheta_D^2}$$

In the discussion species fraction, $\boldsymbol{n_i}$, will be estimated assuming a given $\boldsymbol{f_i}$ factor from the relative intensity $\boldsymbol{A_i}$ of the Mössbauer absorption using $\boldsymbol{n_i = A_i/f_i}$.

Electrochemical tests

The cells consisted of lithium disks (anode) and pellets of wüstite $Fe_{1-x}O$ samples (diameter = 7 mm, thickness ~ 0.3 mm) (cathode), and we used 2 Whatman separators wetted by $LiPF_6$ (1M) electrolyte in PC-EC-3DMC. Charge/discharge curves were carried out galvanostatically by means of a MacPile™ system operating at a current density of 10 A/kg (C/15 rate) between 3 and 0 V vs. Li. Some cells have been stopped at a given depth of discharge or charge, disassembled in a glove box to avoid air and/or moisture contamination.

RESULTS

Pristine material

$Fe_{1-x}O$ has a rocksalt structure (B1, fcc, Fm-3m, a = 4.307 Å [31]). The X-ray diffraction pattern of the pristine material (Fig. 1) presents diffraction of $\theta_{(111)}$ = 18.03, $\theta_{(200)}$ =

20.92, $\theta_{(220)}$ = 30.38, $\theta_{(311)}$ = 36.32 and $\theta_{(222)}$ = 38.14. The refined cell parameter is a = 4.313(7) Å in agreement with the literature. From Aubry and Marion's work [11], the estimated amount of vacancies from the cell parameter is x = 0.050±0.013. Our sample presents some α-Fe impurity (A2, bcc, Im-3m, a = 2.8665 Å [32]) with diffraction peaks of $\theta_{(110)}$ = 22.34, $\theta_{(200)}$ = 32.54, $\theta_{(112)}$ = 41.18. The cell parameter has been roughly evaluated to a = 2.867(8) Å in agreement with the literature.

The ^{57}Fe Mössbauer spectrum shown in Figure 2 presents 3 broadened doublets with an isomer shift IS ~ 1 mm/s and quadrupole splitting ranging from QS ~ 0.50 to QS ~ 1.50 mm/s and their relative areas were corrected from the α-Fe magnetic contribution as described in the experimental part. The absorption intensities are 42, 26 and 15 %. The hyperfine parameters (IS and QS) are rather characteristic of Fe^{II} species involved in wüstite $Fe_{1-x}O$ which is antiferromagnetic (T_N = 198 K [33]) and shows a typical paramagnetic absorption at RT. A fourth doublet centered at IS ~ 0.55 mm/s, QS ~ 0.90 mm/s with a relative area of 11 % is usual of Fe^{III} species as expected in the non-stoichiometric $Fe_{1-x}O$ phase. The estimated amount of vacancies from the Fe^{II}/Fe^{III} ratio as explained in the experimental part is about 0.057±0.008. This value is rather close to 0.050 found from XRD. Finally, the doublet located at IS ~ 0 mm/s and QS ~ 1.68 mm/s, corresponding to α-Fe as explained in the experimental part present a contribution of ~6 %. All these results are summarized in Table 1.

The calculated probabilities P_0, P_1 and P_2 are 50.6, 37.0, 12.4 % for ***x = 0.054*** while the experimental absorptions for Fe^{II} species are 50.7, 31.3 and 18.0 % respectively. The weak discrepancy between calculated P_1 and P_2 and estimated absorptions may suggest that a situation of a Fe^{II} surrounded by 2 Fe^{III} would be most favorable situation than only 1 Fe^{III} in the Fe^{II} neighborhood. This is a small deviation to a random distribution and could indicate of tendency for defect ordering.

Combining XRD and ^{57}Fe Mössbauer spectroscopic results, we can concluded that our pristine sample is mainly (~94 %) composed of $\mathbf{Fe^{II}_{0.838}Fe^{III}_{0.108}\square_{0.054}O}$ and **α-Fe** (~6 %).

Lithiated samples

The electrochemical behavior of $Fe_{1-x}O$ is shown in Figure 3. Starting from the pristine material (point (a) in Fig. 3), the first discharge with a capacity of ~800 Ah/kg is characterized by a pseudo-plateau starting at 0.64 V continuously decreasing to 0.5 V until an uptake of 1 Li (point (b) in Fig. 3), then becomes more sloppy to reach 0.01 V for 2.16 Li (point (c) in Fig. 3). The shape of this not-well defined plateau is rather characteristic for a reconstructive reaction within the pristine material inducing the formation of new phases. The curve of the first charge presents slight different shape with a mean potential of about 1.64 V. At the end of charge (point (d) in Fig. 3), the potential was stopped at 3 V before starting a new cycle for which the Li uptake is 0.94. The difference between discharge and charge (2.16-0.94 = 1.22 Li) results in an irreversible capacity of about 350 Ah/kg. Then next discharge curve shows a very different shape, more sloppy, as compared to the first one. It suggests the formation of new phases or in a more divided state reacting at a mean potential of about 0.98 V. A high polarization of about 660 mV is observed and seems to confirm the nano-structuration of the primary particles during the first discharge. This situation is typical for conversion reactions as described by J.-M. Tarascon *et al.* [34] for oxides, phosphides [35, 36], stannides [37, 38], and antimonides [39, 40]. The following cycles present a rather stable and reversible capacity of about 450 Ah/kg ($\Delta x \sim 1.20$ Li).

Following the establishment of the electrochemical mechanism will only cover the first cycle studied by *ex situ* XRD and ^{57}Fe Mössbauer spectroscopy at points (a)-(d).

X-ray diffraction patterns for the *ex situ* lithiated samples are shown in Figure 4. Depending on the discharge depth we clearly see a progressive consumption of pristine $Fe_{1-x}O$

(Fig. 4a). Nevertheless a rather broadened pattern is observed at the end of the discharge (Fig. 4c), with residual peaks belonging to un-reacted $Fe_{1-x}O$. At this stage, diffraction peaks of α-Fe are still visible, but with a large decrease in intensity compared to the pristine material. Some rather broadened diffuse lines located at around 20-25, 30-33 and 37-42 are also visible and increase in intensity from (b) to (c). This result suggests the formation the new amorphous or nano-sized phases with smaller coherence lengths.

At the end of the first charge (Fig. 4d) the diffraction pattern presents no more crystallized phase. Since $Fe_{1-x}O$ may be reduced to metallic Fe, we have plotted for comparison in Fig. 4d indexations of some known allotropic forms, i.e. α-Fe (bcc), γ-Fe (fcc) and ε-Fe (hcp).

Ex situ Mössbauer spectra of some discharge/charge depths are shown in Figure 5. We have chosen to show the spectra in a wide velocity scale including the total contribution of α-Fe for comparison between the pristine (Fig. 5a) and the fully discharged sample (Fig. 5c). Spectra are rather complex with various components but the overall trend in the shape of the spectra assumes formation of Fe^{III} species upon discharge. The results of the fit have been reported in Table 1.

For an uptake of 1 Li (Fig. 5b), we observed in the spectrum a decrease for the Fe^{II} contribution and an increase for Fe^{III} (IS ~ 0.5 mm/s, QS ~ 0.66 mm/s). Hyperfine parameters (IS and QS) differ slightly from Fe^{III} species in the pristine material. This Fe^{III} contribution is not only due to Fe^{III} in $Fe_{1-x}O$, but it could be nano-sized $Fe^{III}_2O_3$ which can be superparamagnetic if the particle size is small as we assume. It is worth to notice that in $Fe_{1-x}O$ some local defects are ordered giving Koch-Cohen clusters ($V_{13}T_4$ type or $V_{16}T_5$) with a composition close to magnetite Fe_3O_4 [41, 42].

The contribution of α-Fe also increases in intensity with IS ~ 0.02 mm/s and QS ~ 1.675 mm/s. We have freed these two parameters in the fitting procedure to obtain

convergence. Although this is within the error bars, it could be significant if we consider that new α-Fe is formed with smaller particles, resulting in a slightly modified hyperfine magnetic field with a shifted spectrum. We also observe the formation of a rather broadened (Γ = 0.6 mm/s) singlet located at negative velocity (IS = -0.054 mm/s). It cannot be associated to α-Fe in micro-particles because in this case it must conserve its hyperfine magnetic field even at room temperature. It could be due to the presence of superparamagnetic Fe nano-particles with a size smaller than 2 nm [43]. This isomer shift is generally observed at room temperature in the case of paramagnetic spectra of austenitic steels. It could be associated to the formation of γ-Fe (fcc, Fm-3m, a = 3.587 Å). It is well established that γ-Fe is paramagnetic in a nonferromagnetic state at RT [44]. We know also a diffusive transition transforming α-Fe into γ-Fe occurs at 912 °C. We don't really believe that the signal observed can be reasonably attributed to γ-Fe. It is not excluded that ε-Fe (A3, hcp, $P6_3/mmc$) is formed [45, 46]. Indeed these two allotropic forms (γ and ε) differ only by the stacking sequences (ABCABC) and (ABABAB), respectively. On the other hand, at high pressure and room temperature α-Fe becomes ε-Fe in a martensitic phase transition [47, 48]. Anyway the broadened singlet could be attributed to either α-Fe (bcc) or ε-Fe (hcp) in nano-particles. In the doubt, we prefer to call this metallic fingerprint nano-Fe^0 as mentioned in Table 1.

These results suggest that the active material $Fe_{1-x}O$ reacts while new divided metallic Fe is formed with a new species containing Fe^{III}. Surprisingly, we can assume at this stage the disproportionation of $3Fe^{II}$ into $2Fe^{III}$ and $1Fe^0$.

As previously explained, from the relative areas of Fe^{II} species with found a vacancies amount of $\boldsymbol{x = 0.036}$. The proposed formula for wüstite at this depth of discharge is $\mathbf{Fe^{II}_{0.892}Fe^{III}_{0.072}\square_{0.036}O}$.

At the end of the discharge for an uptake of 2.16 Li (Fig. 5c), ~23 % of the absorption belongs to Fe^{II} species. Hence, $Fe_{1-x}O$ does not completely react. The Fe^{III} species

contribution decreases from ~12 % (1 Li) to ~6 %. At this stage the increase in size of Fe_2O_3 particles induces a transition in the Mössbauer spectra from a superparamagnetic (doublet) to a magnetic (sextet) contribution. At RT this transition occurs for a particle size around 15 nm for hematite (K_{eff} ~1 $kJ.m^{-3}$) [49]. Metallic iron (micro and nano) contribution increases from ~25 to ~31 %. From the relative area of the Fe^{II} species with ***x = 0.032***, the proposed formulae for wüstite at this depth of discharge is $\mathbf{Fe^{II}_{0.904}Fe^{III}_{0.064}\square_{0.032}O}$.

All along the discharge by comparing XRD and Mössbauer spectroscopic data analysis we can propose the following: i) the active material $Fe_{1-x}O$ reacts partially with Li forming a phase containing Fe^{III} (Fe_2O_3), ii) starting from Fe^{II}, the production of Fe^{III} must be necessarily accompanied by the production of Fe^0 (disproportionation), iii) a not well understood broadened singlet with negative velocity could be a nano-sized Fe, and iv) vacancies are progressively filled or used by Li during the transformation of FeO forcing Fe atoms to quit the structure.

Finally at the end of the charge (Fig. 5d), we observe a contribution of ~66 % for Fe^{II}, ~4 % for Fe^{III} and ~30 % Fe^0. Metallic iron particles became less than 2 nm in size since no magnetic sextet of α-Fe is observed, we can assume that it plays a role during the Li extraction mechanism. Form the relative area of Fe^{II} species with ***x = 0.062***, the proposed formulae for wüstite at this depth of discharge is $\mathbf{Fe^{II}_{0.814}Fe^{III}_{0.124}\square_{0.062}O}$.

A correlation between the quadrupole splitting of the Fe^{II} sites and the number of Fe^{III} ***n*** in the Fe^{II} neighborhood has been found: ***QS(n) = 0.502 + 0.491 n*** for the pristine material and ***QS(n) = 0.569 + 0.467 n*** for a depth of discharge of 1 Li. These two tendencies are very close and the slight deviation between intercepts and slopes may be correlated to the amount of vacancies in both compositions. The correlation we found at the end of the first charge is ***QS(n) = 0.3 + 0.576 n***. This tendency is very different to those previously estimated at the discharge. This result suggests that the conversion reaction deeply modifies the Fe^{II}

environment. It is worth to note that the isomer shift is also affected, decreasing from about 1 mm/s at the discharge to ~0.7±1 mm/s at the end of the charge.

DISCUSSION

A concept previously introduced by Connerade *et al.* [50] and described as an "electronic pressure" at atomic level (Hartree-Fock calculations) confirms that electrochemical lithium reaction acts as an increase of pressure [51, 52]. It is worth noticing that lithium-based electrochemical reactions present some analogies with high-pressure studies: oxidation state change, phase transition, amorphization, volume collapse. In the case of oxides, the pressure may induce valence state transitions, structural transitions and in some cases amorphization of the compound [53, 54]. For instance, Fe_2O_3 plays a determining role in the understanding the physical properties of the Earth's mantle [55]. At high-pressure Fe_2O_3 undergoes an oxidation state transformation from Fe^{3+} to a new valence state [56]. The same behavior has been observed for the disproportionation of SnO into β-Sn and SnO_2 [57]. Recently, the disproportionation of wüstite ($Fe_{1-x}O$) has attracted increasing attention, as a mechanism for the formation of metallic iron in the origin of the chemical differentiation of planetary materials [58, 59]. In this latter case from $Fe^{II}_{0.805}Fe^{III}_{0.13}\square_{0.065}O$, the authors found about 4.8 % of metallic iron are irreversibly formed at high-pressure with 95.2 % of $Fe^{II}_{0.655}Fe^{III}_{0.23}\square_{0.115}O$ [60].

At room temperature, metallic iron and tin present a well established martensitic phase transition from α-Fe (bcc) to ε-Fe (hcp) and from β-Sn (bct) to Sn-II (bcc) at about 10.0 and 9.2 GPa respectively [61, 62]. Besides the structural phase transition, an important change in the magnetic properties of the iron atoms is found: namely iron which is ferromagnetic in the α phase becomes nonmagnetic in the ε phase [63]. The interest in high-pressure (HP)

behavior of elemental iron primarily stems from the fact that the hexagonal closed packed (hcp) phase of iron (ε-Fe) is considered as major constituent of the Earth's inner core [64]. Results obtained under HP by ^{57}Fe Mössbauer spectroscopy clearly show a reduced atomic density in the boundary regions [65].

The effect of hydrostatic pressure isomer shift (IS) has been the subject of extensive research [66, 67]. These changes of IS in Mössbauer effect measurements are proportional to those in "s"-electron density ρ_v (0) at the nuclei in an absorber or a source. Variation of ρ (0) in compressed metals, alloys, and compounds is seen to involve several mechanisms, whose relative weight dictates the corresponding volume dependence. The main factors affecting the density of the ns electrons are: (i) reduction of the lattice parameters [68], (ii) screening of the 5p (^{119}Sn, ^{121}Sb, ^{125}Te) or 4d (^{57}Fe) electrons [69].

In our case, the electrochemical lithium reaction induces an amorphization of the $Fe_{1-x}O$ active material or a formation of metallic nano-particles as shown by XRD. In our ^{57}Fe Mössbauer data we have a signature of some nanosized-Fe with an isomer shift IS = -0.054 mm/s which corresponds to metallic iron at a pressure of 6.7 GPa [65]. The line width is also pressure-sensitive, we found Γ = 0.6mm/s which is consistent to ε-Fe at 14 GPa [45, 70]. It seems that in our material, the metallic iron particles are formed at a scale around 2 to 10 nm since we have coexistence of some magnetic α-Fe and superparamagnetic nano-particles. These particles are more or less compressed by the Li_2O matrix. ^{57}Fe Mössbauer spectra also give in our case more information in terms of vacancies. These vacancies play a role for cation diffusion in the FeO structure.

We propose the following electrochemical mechanism occurring upon Li reaction for the first discharge:

1) $(\alpha-3\beta)\ Fe^{II}O + 2(\alpha-3\beta)\ Li \rightarrow (\alpha-3\beta)\ Fe^{0} + (\alpha-3\beta)\ Li_2O$ (reduction)

2) $3\beta\ Fe^{II}O \rightarrow \beta\ Fe^{0} + \beta\ Fe_2^{III}O_3$ (disproportionation)

From the data summarized in Table 1, we found $\alpha = 0.256$ and $\beta = 0.0215$ between points (a) and (b) in Fig. 5 and $\alpha = 0.549$ and $\beta = 0.0315$ between points (a) and (c) in Fig. 5. These values mean that about 26 % of FeO is consumed during the first part. During the last part of the discharge curve, 29 % of FeO is consumed. Some active FeO material (~40 %) did not react. There is a concomitant reduction (reaction 1) and disproportionation (reaction 2). Concerning the structural modification involved in such a mechanism, the Li applies some "electronic pressure" forcing diffusion of Fe ions. This increase of internal pressure induces Fe extrusion out from the FeO structure in which formation of vacancies forming small clusters of $Fe_2\square O_3$. At the end of the discharge, it is more and more difficult to force Fe to quit the wüstite structure and these clusters are growing giving magnetic Fe_2O_3 nanoparticles. To summarize the electrochemical mechanism during the discharge we have:

$$\mathbf{0.549\ Fe^{II}O + 0.909\ Li \rightarrow 0.486\ Fe^{0} + 0.4545\ Li_2O + 0.0315\ Fe_2O_3},$$

Compared to the electrochemical curve (Fig. 3) we clearly see that ~1.25 Li are missing although 2.16 Li were consumed for the global reaction. It suggests that ~58 % of Li is used for SEI formation at the surface of the electrode material and is not directly involved in the redox process. This SEI is at the origin of the irreversible capacity in the conversion reaction [71]. Apart from the charge consumed for the reduction of the solvent, this SEI is also believed to enable additional lithium storage on its surface in metallic form [72]. Any way, it has been shown that using nano-particle electrodes, electrolyte decomposition may occur simultaneously to the conversion reaction [73].

At the charge, starting from 2.16 Li, we extract about (2.16-0.94) = 1.22 Li. The electrochemical mechanism deduced from Mössbauer data analysis is for the charge:

$$\mathbf{0.230\ Fe^{0} + 0.2285\ Li_2O + 0.0015\ Fe_2O_3 \rightarrow 0.233\ Fe^{II}O + 0.457\ Li}$$

Here again ~63 % of extracted Li are used for SEI consumption. It means that only ~50 % of the formed SEI during the first discharge is consumed during the first charge. Our observations are in agreement with previous works based on the lithium conversion reaction of the 3d transition-metal oxides such as CoO [74] and NiO [75], which can be reversibly reduced and oxidized, coupled with the formation and destruction of lithium oxide, respectively.

In Figure 6 we have plotted the relative amount n_i deduced from Mössbauer data analysis of the species upon Li reaction during the first discharge up to 2.16 Li and the first charge stopped at 0.94 Li. After the middle of the first discharge, particles of α-Fe^0 progressively decrease in size and transforms into nanosized Fe^0. During the charge only a part of this nano-Fe^0 can reversibly react to form highly divided FeO. This is in agreement with the first derivative electrochemical curve shown in Figure 7. We have decomposed the observed shape into the sum of 2 or 3 Gaussian functions. The 1st discharge is composed of 3 peaks with a position, a width and a surface of (0.57 V, 70 mV, 29 %), (0.48 V, 135 mV, 35 %) and (0.30 V, 268 mV, 36 %) respectively. If we assume that these surfaces are proportional to the number of Li involved in a reaction, the very first one peak corresponds to about ~0.63 Li. The width of this peak is very thin and is a signature of a two-phase mechanism. It corresponds to the main reaction $FeO + 2Li \rightarrow Fe + Li_2O$. The end of the first discharge involves rather broadened peaks suggesting SEI growth. During the first charge a broadened peak located at about 1.31 V should correspond to SEI consumption while the thin peak at 1.64 V may correspond to nanoFe^0 oxidation into FeO (~44 % compared to 37 % of Li). At the second discharge we found a thin peak (ΔV ~ 47 mV) located at 0.98 V. Assuming the reversible reaction shows a rather high polarization of about 1.64-0.98 = 660 mV due to highly divided material.

CONCLUSION

Electrochemical lithium conversion reaction of FeO wüstite has been investigated using X-ray diffraction and Mössbauer spectroscopy. Detailed analysis of Mössbauer spectra suggests that vacancies play a role in cation diffusion. These results reveal that *in situ* formation of nanometric metallic iron particles with a size smaller than 2 nm embedded in a Li_2O matrix is accompanied with some traces of Fe_2O_3 that growth to reach a size of about 15 nm. This suggests that Fe^{III} defect in the FeO structure may be close to each other to permit small amounts of Fe_2O_3 to reach rather high size compared to metallic iron nanoparticles. Therefore, a very high metal/Li_2O interface induces an increase of pressure detected through isomer shift and quadrupole splitting variations. Upon reoxidation of these nanocomposites, very small clusters of oxides are formed back since hyperfine parameters of FeO are different compared to the pristine material. However, the formation of such nanocomposites should now be investigated using *in situ* and *operando* ^{57}Fe Mössbauer spectroscopy in order to follow global absorption of the sample to have a better estimation of the Lamb-Mössbauer factor of metallic nanoparticles [37]. In that case 2D correlation analyses of numerous recorded spectra would provide more precise information on the electrochemical mechanism as done on iron-based cathode materials [12].

TABLES

Table 1. Isomer shift (IS), quadrupole splitting (QS), relative areas (A%), assignment and corrected areas from metallic iron magnetic sextet. The star (*) corresponds to inner lines 3 and 4 of the sextet of magnetic spectrum for α-Fe. Since spectra have been recorded in a small velocity range (±2.4 mm/s), the estimated area for the lines 3 and 4 has to be multiplied by 6 respecting the expected intensity ratios 3:2:1:1:2:3. Estimated relative population of the species n_i is given assuming Lamb-Mössbauer factors: $f_{FeO} \sim f_{\alpha\text{-}Fe} = 0.79$, $f_{FeIII} = 0.81$ and $f_{nanoFe} = 0.51$. Proposed assignments are given. Relative contributions of most probable Fe^{II} environments (see text) are given compared to the calculated probabilities $P_n = P_{n,0} + P_{n,1} + P_{n,2}$ for Fe^{II} environments determined from ^{57}Fe Mössbauer spectra for the pristine material and after various discharge/charge depths. In $P_{n,m}$, n stands for the number of Fe^{III} first neighbors and m the number of vacancies. The vacancies amount is given by x in the formula $Fe^{II}_{1-3x}Fe^{III}_{2x}\square_x O$.

Pristine material $Fe_{1-x}O$				
IS (mm/s)	QS(mm/s)	A, $\mathbf{A_c}$, n_i	Assignment	A%, P_n
1.021	0.518	43.9, **42.2,** *42.3*		50.7, *50.6 (n=0)*
0.998	0.961	27.1, **26.1,** *26.2*	Fe^{II} in	31.3, *37.0 (n=1)*
1.049	1.500	15.6, **15.0,** *15.0*	$Fe^{II}_{1-3x}Fe^{III}_{2x}\square_x O$	18.0, *12.4 (n=2)*
0.549	0.905	11.4, **10.9,** *10.7*	Fe^{III} in $Fe^{II}_{1-3x}Fe^{III}_{2x}\square_x O$	*x=0.054*
0.00*	1.68*	2, **5.8,** *5.8*	$\alpha\text{-}Fe^0$	
After insertion of **1 Li** in $Fe_{1-x}O$				
IS (mm/s)	QS(mm/s)	A, $\mathbf{A_c}$, n_i	Assignment	A%, P_n
0.993	0.576	46.9, **39.4,** *38.4*		62.2, *62.2 (n=0)*
0.937	1.020	19.7, **16.5,** *16.1*	Fe^{II} in	26.0, *30.8 (n=1)*
1.035	1.509	9.0, **7.5,** *7.3*	$Fe^{II}_{1-3x}Fe^{III}_{2x}\square_x O$	11.8, *7.0 (n=2)*
0.514	0.657	14.0, **11.7,** *6.8+4.3*	$Fe^{III}_{superpara}Fe_2O_3$	*x=0.036*
0.021*	1.675*	23.1, **19.4,** *18.9*	$\alpha\text{-}Fe^0$	
-0.054	-	6.5, **5.5,** *8.2*	Fe^0_{nano}	
After insertion of **2.16 Li** in $Fe_{1-x}O$				
IS (mm/s)	QS(mm/s)	A, $\mathbf{A_c}$, n_i	Assignment	A%, P_n
0.688	0.435	19.5, **13.9,** *15.8*	Fe^{II} in	40.2, *39.9 (n=0)*
1.030	0.497	17.1, **12.2,** *13.9*	$Fe^{II}_{1-3x}Fe^{III}_{2x}\square_x O$	35.4, *40.9 (n=1)*
1.151	0.839	11.8, **8.4,** *9.6*		24.4, *19.2 (n=2)*
0.661*	2.650*	8, **5.7,** *6.3*	$Fe^{III}_2O_3$	*x=0.072*
-0.024	-	43.6, **31.1,** *54.4*	Fe^0_{nano}	
After lithium extraction (end of first charge)				
IS (mm/s)	QS(mm/s)	A, $\mathbf{A_c}$, n_i	Assignment	A%, P_n
0.665	0.305	28.0, **23.3,** *24.7*		39.4, *39.9 (n=0)*
0.746	0.866	30.3, **25.3,** *26.8*	Fe^{II} in	42.8, *40.9 (n=1)*
0.877	1.457	12.6, **10.5,** *11.1*	$Fe^{II}_{1-3x}Fe^{III}_{2x}\square_x O$	17.8, *19.2 (n=2)*
0.661*	2.650*	4, **3.3,** *3.4*	$Fe^{III}_2O_3$	*x=0.072*
0.041	-	25.1, **20.9,** *34.0*	Fe^0_{nano}	

FIGURES

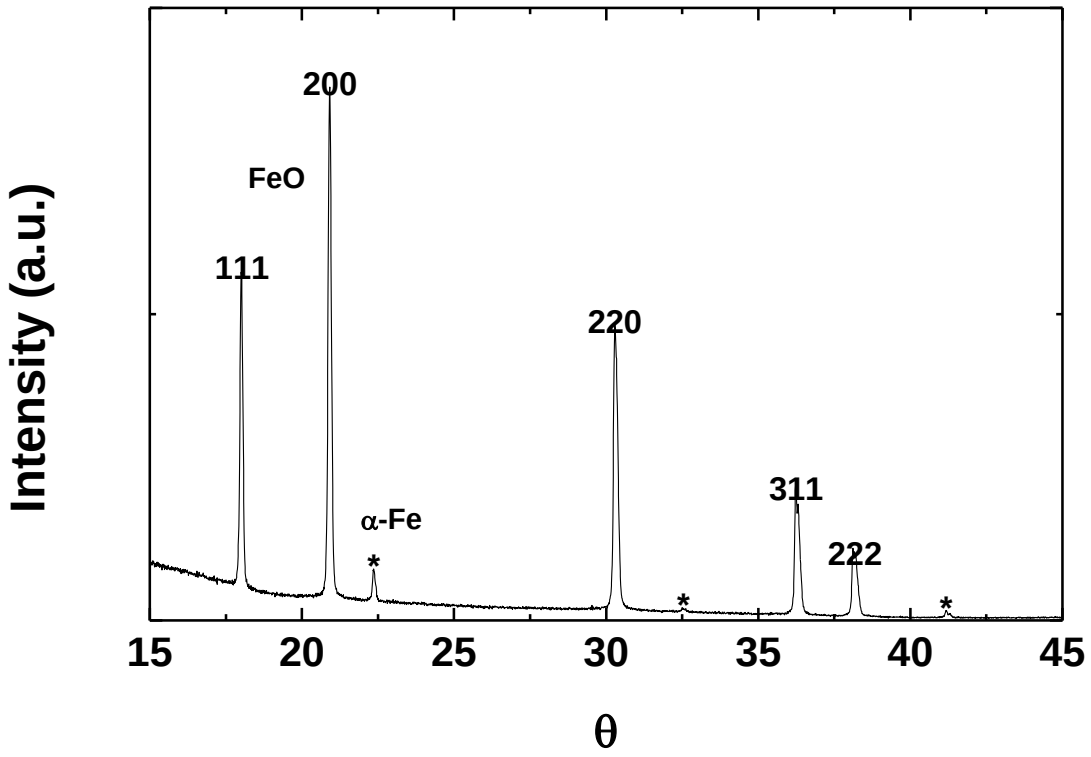

Figure 1: X-ray diffraction pattern of the pristine $Fe_{1-x}O$ material recorded using Cu-Kα radiation. From indexed lines cell parameter is a_{FeO} = 4.313(7) Å. (*) α-Fe as impurity with bcc lattice and cell parameter $a_{\alpha\text{-}Fe}$ = 2.867(1) Å.

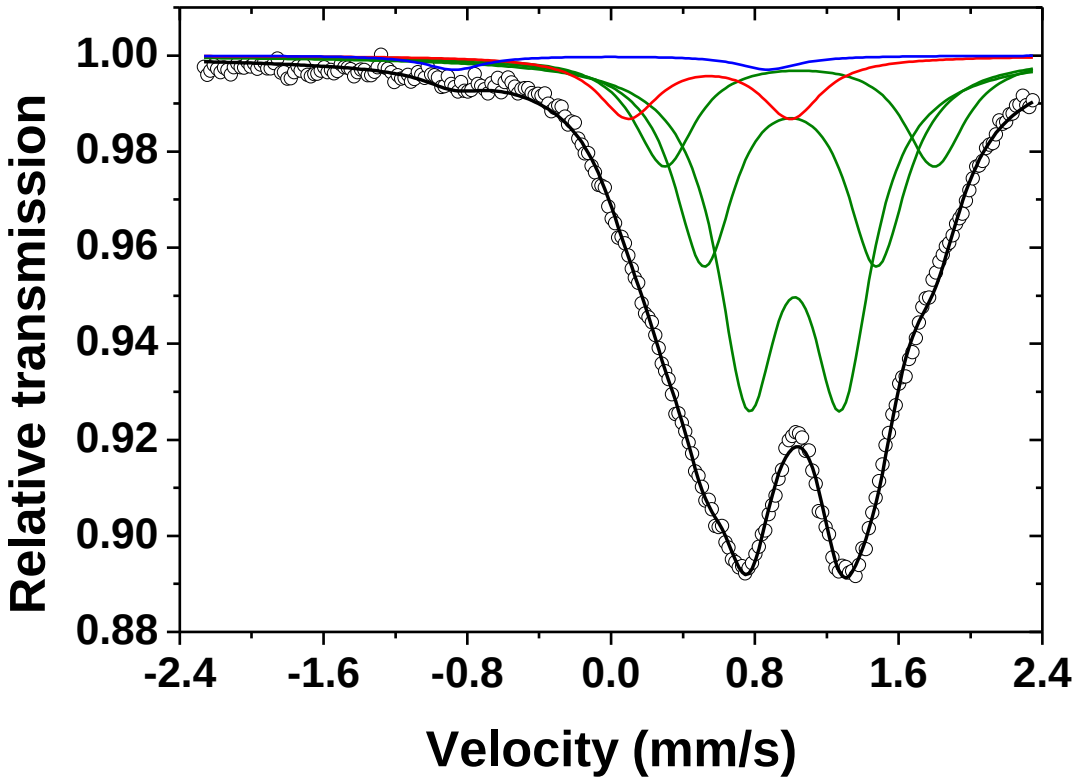

Figure 2: ^{57}Fe Mössbauer spectrum at 300 K of the pristine $Fe_{1-x}O$ material. Three doublets centered at about 1 mm/s are inferred to Fe^{II} and the doublet centered at 0.55 mm/s lies in the range of Fe^{III}. The areas of the 3 doublets of Fe^{II} are in the ratio 51:31:18. The impurity (2 %) of the overall absorption is characterized by a doublet centered at δ = 0 mm/s with Δ = 1.68 mm/s corresponding to inner lines 3 and 4 of the sextet of to α-Fe as impurity.

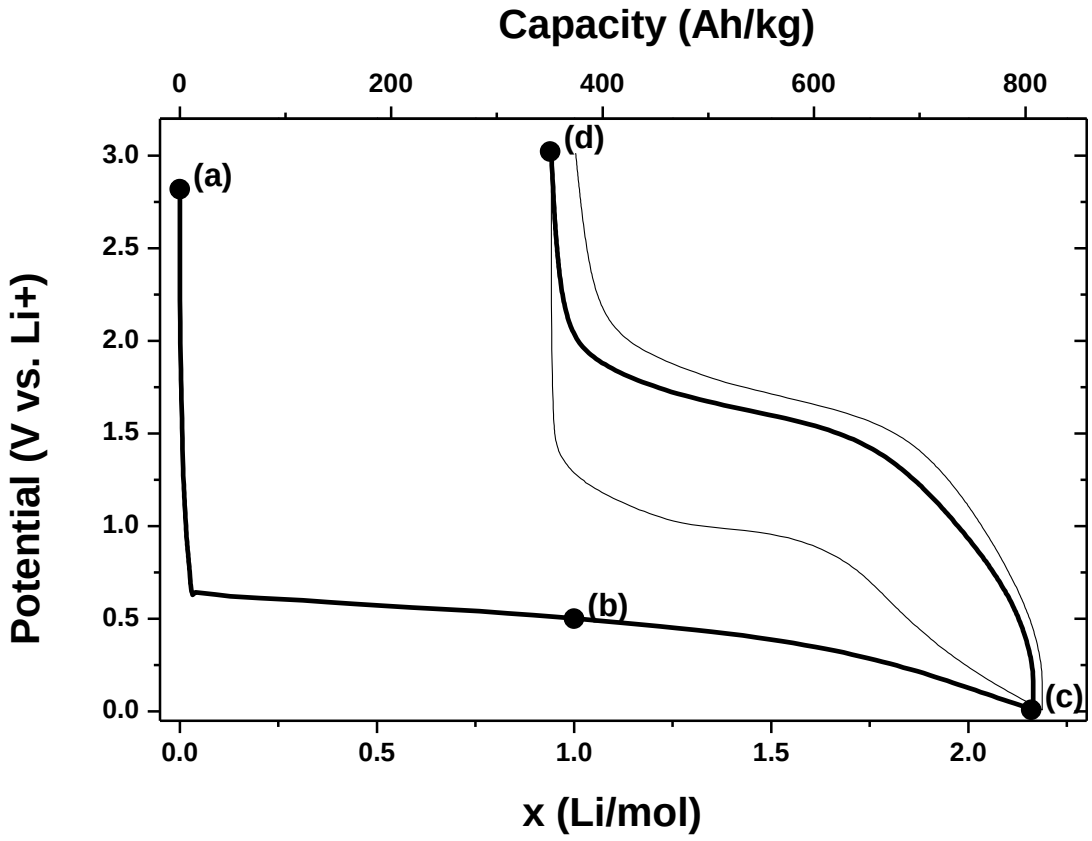

Figure 3: Discharge-charge curves of Li insertion in $Fe_{1-x}O$ wüstite compound. Solid labeled circles correspond to samples characterized by ^{57}Fe Mössbauer spectroscopy and X-ray diffraction for a given depth of discharge/charge. The first (second) discharge-charge cycle is represented in bold (thin) line.

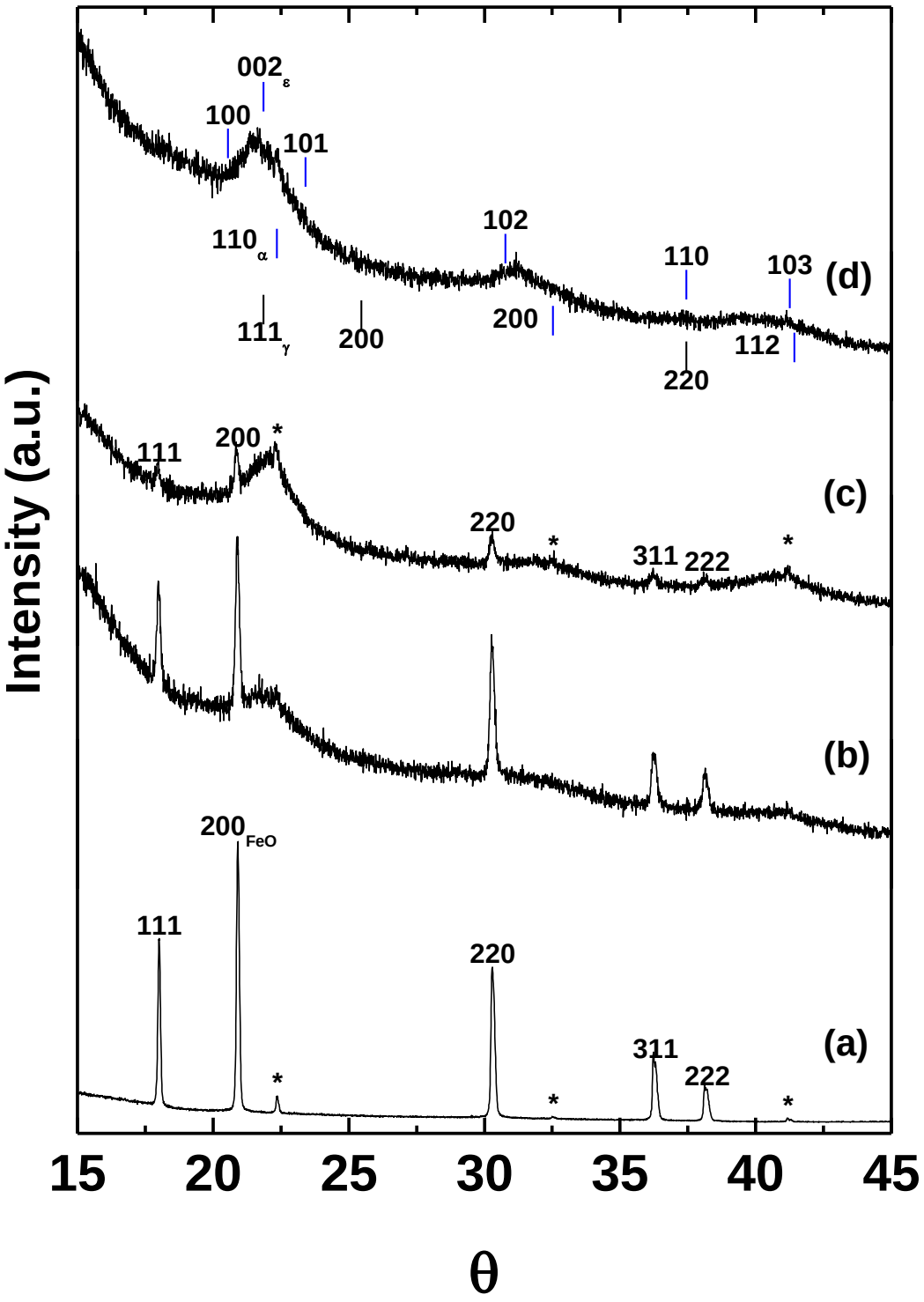

Figure 4: Comparison of X-ray diffraction patterns of the pristine $Fe_{1-x}O$ material (a) with small impurity of α-Fe (*), after insertion of 1 Li (b) and the end for discharge at 2.2 Li (c). Label (d) corresponds to the end of the first charge at 1 Li. Indexation is given for FeO; α-Fe is still present during the first discharge. Indexation for the 3 allotropic forms of metallic iron is given on the pattern (d): α-Fe (bcc), γ-Fe (fcc), ε-Fe (hcp). For ε-Fe, indexation is represented above the pattern and positions are in the rather good agreement with the observed broadened peaks.

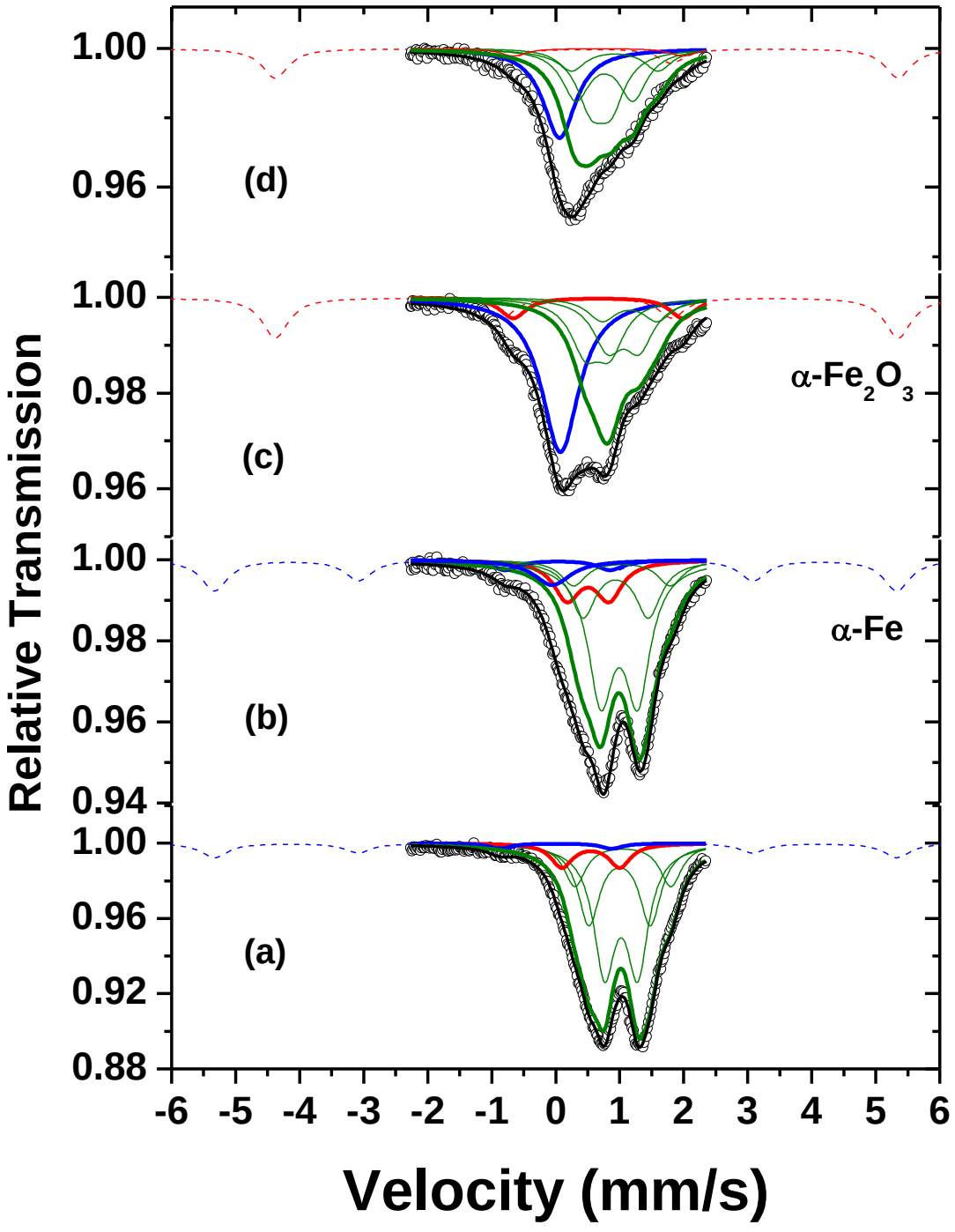

Figure 5: Comparison of ^{57}Fe Mössbauer spectra at 300 K of the pristine $Fe_{1-x}O$ material (a), after an uptake of 1 Li (b) and the end for discharge at 2.16 Li (c). Green contributions are attributed to Fe^{II}. The thicker green line is sum of the thinner one corresponding to unreacted $Fe_{1-x}O$. Dashed blue line corresponds to the expected increasing contribution of α-Fe from (a) to (c). In the case of (c), magnetic sextet has been slightly shifted as a guide of the eye. Spectrum (d) corresponds to the end of the first charge at 0.94 Li with no α-Fe contribution, but the blue singlet nanosized metallic ε-Fe^0 is still present.

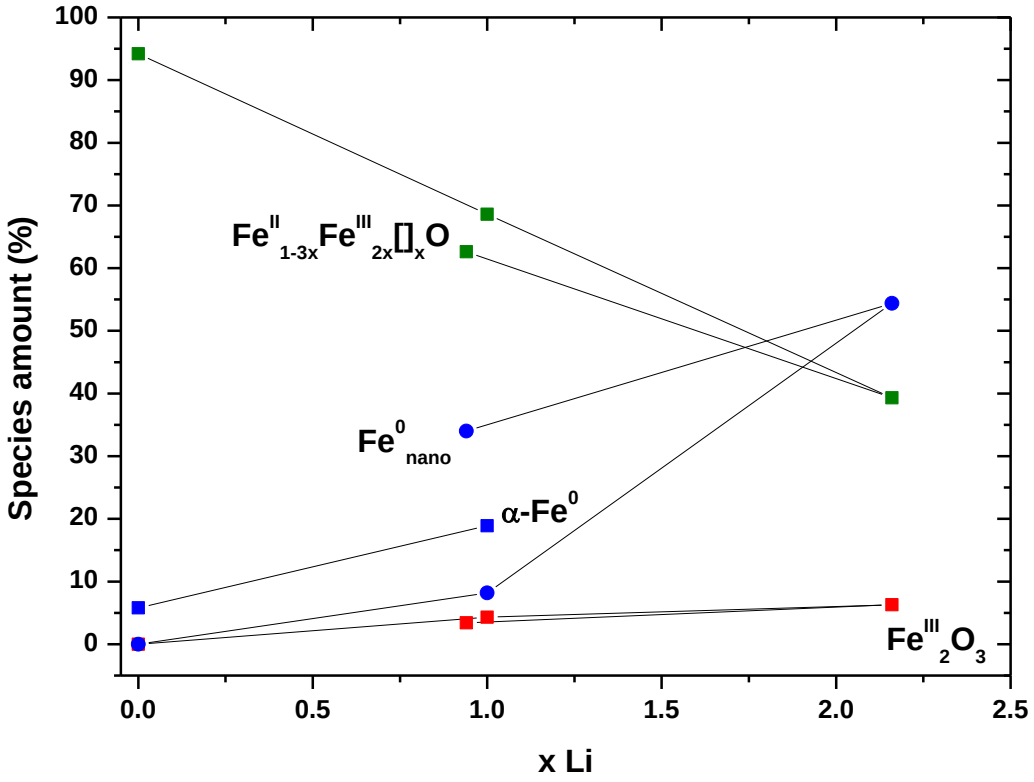

Figure 6: Evolution of the relative amount of species upon Li reaction during the first discharge (2.16 Li) and charge (stopped at 0.94 Li). After the middle of the first discharge, α-Fe^0 progressively transforms into Fe^0_{nano}. During the charge only a part of nano-Fe^0 can react to form FeO.

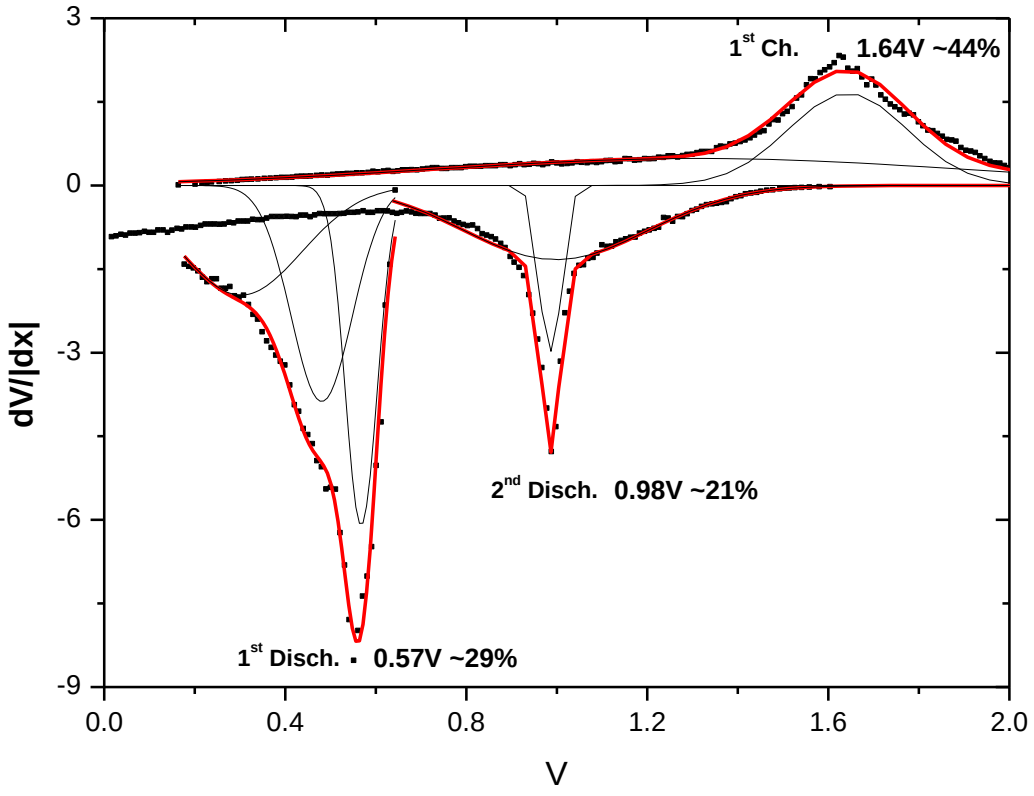

Figure 7: Details of the first derivative of the electrochemical curve along the first and second discharge and along the first charge. The thinner peaks at the 1st and the 2nd discharge located at 0.57 V and 0.98 V represent about 29 % and 21 % of the surface respectively. During the charge the rather thick peak located at 1.64 V represents ~44 % of the surface.

REFERENCES

[1] A. De Guibert, Lettre des Sciences Chimiques, L'Actualité Chimique 3 (1998) 15-17.
[2] D. Guyomard, Lettre des Sciences Chimiques, L'Actualité Chimique 7 (1999) 10-18.
[3] M.M. Thackeray, W.I.F. David, J.B. Goodenough, Mater. Res. Bull. 17 (1982) 785-793.
[4] B.D. Pietro, M. Patriarca, B. Scrosati, J. Power Sources 8 (1982) 289-299.
[5] N.A. Godshall, I.D. Raistrick, R.A. Huggins, Mater. Res. Bull. 15 (1980) 561-568.
[6] D. Larcher, C. Masquelier, D. Bonnin, Y. Chabre, V. Masson, J.B. Leriche, J.M. Tarascon, J. Electrochem. Soc. 150 (2003) A133-139.
[7] J. B. Goodenough, Progress in Solid State Chemistry 5 (1971) 145-399.
[8] L. Dupont, S. Grugeon, S. Laruelle, J-M. Tarascon Journal of Power Sources 164 (2007) 839-848.
[9] C. A. McCammon, L.-G. Liu, Phys. Chem. Minerals 10 (1984) 106-113.
[10] B. Hentschel B., Z. Naturforsch. 25 (1970) 1996-1997.
[11] J. Aubry, F. Marion, C. R. Acad. Sci. Paris 241 (1955) 1778-1781.
[12] L. Aldon, A. Perea, J. Power Sources 196 (2011) 1342-1348.
[13] P. Kubiak, A. Garcia, M. Womes, L. Aldon, J. Olivier-Fourcade, P.-E. Lippens, J.-C. Jumas, J. Power Sources 119-121 (2003) 626-630.
[14] L. Aldon, M. Van Thournout, P. Strobel, O. Isnard, J. Olivier-Fourcade, J.-C. Jumas, Solid State Ionics 177 (2006) 1185-1191.
[15] L. Aldon, J. Olivier-Fourcade, J.-C. Jumas, M. Holzapfel, C. Darie, P. Strobel, J. Power Sources 146 (2005) 259-263.
[16] P. C. Hayes, Metallurgical and Materials Transactions B 41 (2010) 19-34.
[17] L. S. Darken, R. W. Gurry, Am. Chem. Soc. 67 (1945) 1398-1412.
[18] A. Hoffmann, Z. Elektrochemie 63 (1959) 107-213.
[19] K.Ruebenbauer, T.Birschall, Hyperfine Interactions 7 (1979) 125-127.
[20] S.L.Ruby, Mössbauer Effect Methodology 8 (1973) 263-276.
[21] M. Womes, F. Py, M. L. Elidrissi Moubtassim, J. C. Jumas, J. Olivier-Fourcade, F. Aubertin, U. Gonser, J. Phys. Chem. Solids 55 (1994) 1323-1329.
[22] S. Sen and C. A. Russell, T. Mukerji, Phys. Rev. B 72 (2005) 174205-174212.
[23] G. Rixecker, Hyperfine Interactions 130 (2000) 127-150.
[24] I. Kantor, L. Dubrovinsky, C. McCammon, G. Steinle-Neumann, A. Kantor, N. Skorodumova, S. Pascarelli, G. Aquilanti, Phys. Rev. B 80 (2009) 014204-014215.
[25] A. Van Alboom, V. G. De Resende, E. De Grave, J. A. M. Gómez, J. Mol. Struc. 924–926 (2009) 448-456.
[26] J.S. van Wieringen, Phys. Lett. 26A (1968) 370-371.
[27] L. Aldon, A. Perea, M. Womes, C.M. Ionica-Bousquet, J.-C. Jumas, J. Solid State Chem. 183 (2010) 218-222.
[28] H. Guérault, Y. Labaye, J.-M. Grenèche, Hyperfine Interactions, 136 (2001) 57-63.
[29] J. R. Childress, C. L. Chien, M. Y. Zhou, Ping Sheng , Phys. Rev. B 44 (1991) 11689-11696.
[30] L. Stixrude, C. Lithgow-Bertelloni, Earth Planet. Sci. Lett. 263 (2007) 45-55.
[31] Bragg L., Claringbull G.F. "Crystal structure of minerals", London, G.Bell and Sons LTD (1965).
[32] R.W.G. Wyckoff, Crystal Structures, sec. ed., 1, 15 (1963).

[33] Schiber M. M., ed., Experimental Magnetochemistry, John Wiley & Sons, New York, (1967).
[34] J.-M. Tarascon, S. Grugeon, M. Morcrette, S. Laruelle, P. Rozier, P. Poizot, Comptes Rendus Chimie, 8 (2005) 9-15.
[35] C. Villevieille, M. Boinet, L. Monconduit, Electrochem. Com. 12 (2010) 1336-1339.
[36] H. Pfeiffer, F. Tancret, M.-P. Bichat, L. Monconduit, F. Favier, T. Brousse, Electrochem. Com. 6 (2004) 263-267.
[37] L. Aldon, C.M. Ionica, P.E. Lippens, D. Larcher, J.M. Tarascon, J. Olivier-Fourcade, J.-C. Jumas, Hyperfine Interactions 167 (2006) 729-732.
[38] C. M. Ionica-Bousquet, P. E. Lippens, L. Aldon, J. Olivier-Fourcade, J. C. Jumas, Chem. Mater., 18 (2006) 6442-6447.
[39] L. Aldon, A. Garcia, J. Olivier-Fourcade, J.-C. Jumas, F. J. Fernández-Madrigal, P. Lavela, C. Pérez Vicente, J. L. Tirado, J. Power Sources 119-121 (2003) 585-590.
[40] C. Villevieille, C.-M. Ionica-Bousquet, B. Ducourant, J.-C. Jumas, L. Monconduit, J. Power Sources, 172 (2007) 388-394.
[41] T. R. Welberry, A. G. Christy, Phys Chem Minerals 26 (1998) 81-82.
[42] F. Koch, J.B. Cohen, Acta Cryst. B 25 (1969) 275-287.
[43] P. Tartaj, T. Gonzalez-Carreno, O. Bomati-Miguel, C. J. Serna, P. Bonville, Phys. Rev. B 69 (2004) 094401-094408.
[44] S. Groudeva-Zotova, R. Kozhuharova, D. Elefant, T. Mühl, C.M. Schneider, I. Mönch, J. Magn. Magn. Mater. 306 (2006) 40-50.
[45] D. L. Willamson, S. Bukshpan, R. Ingalls, Phys. Rev. B 6 (1972) 4194-4206.
[46] J.-P. Rueff, M. Mezouar, M. Acet, Phys. Rev. B 78 (2008) 100405-100408(R).
[47] L. Miyagi, M. Kunz, J. Knight, J. Nasiatka, M. Voltolini, H.-R. Wenk, J. Appl. Phys. 104 (2008) 103510-103512.
[48] D. F. Johnson, E. A. Carter, The J. Chem. Phys. 128 (2008) 104703-104709.
[49] F. Bødker, M. F. Hansen, C. Bender Koch, K. Lefmann, S. Mørup, Phys. Rev. B 61 (2000) 6826-6838.
[50] J.P. Connerade, J. Alloys and Compounds, 255 (1997) 79-90.
[51] J.P. Connerade, J.-C. Jumas, J. Olivier-Fourcade, J. Solid State Chem. 152 (2000) 533-536.
[52] J. Olivier-Fourcade, J.-C. Jumas, J.P. Connerade, J. Solid State Chem. 147 (1999) 85-91.
[53] E. G. Ponyatovsky, O. I. Barkalov, Mater. Sci. Rep. 8 (1992) 147-191.
[54] N. Binggeli, N. R. Keskar, J. R. Chelikowsky, Phys. Rev. B 49 (1994) 3075-3081.
[55] S. Ono, T. Kikegawa, Y. Ohishi, J. Phys. Chem. Solids, 65 (2004) 1527-1530.
[56] M.P. Pasternak, G.K. Rozenberg, G.Y. Machavariani, O. Naaman, R.D. Taylor, R.J. Phys. Rev. Lett. 82 (1999) 4663-4666.
[57] H. Giefers, F. Porsch, G. Wortmann, Physica B 373 (2006) 76-81.
[58] E. M. Galimov, Geochem. Int. 36 (1998) 673-675.
[59] D. J. Frost, C. Liebske, F. Langenhorst, C. A. McCammon, R. G. Trønnes, D. C. Rubie, Nature 428 (2004) 409-412.
[60] S. V. Ovsyannikov, V. V. Shchennikov, M. A. Shvetsova, L. S. Dubrovinsky, A. Polian, Phys. Rev. B 81 (2010) 060101-060104 (R).
[61] S. Desgreniers, Y. K. Vohra, A. L. Ruoff, Phys. Rev. B 39 (1989) 10359-10363.
[62] S. Cui, L. Cai, W. Feng, H. Hu, C. Wang, Y. Wang, Phys. status solidi (b) 245 (2008) 53-55.
[63] G. Steinle-Neumann, R.E. Cohen, L. Stixrude, J. Phys.: Condens. Matter 16 (2004) S1109-S1119.
[64] A.K. Singh, A. Jain, H.P. Liermann, S.K. Saxena, J. Phys. Chem. Solids 67 (2006) 2197-2202.

[65] S. Trapp, C.T. Limbach, U. Gonser, S.J. Campbell, H. Gleiter, Phys. Rev. Lett. 75 (1995) 3760-3763.
[66] E. Ratner, M. Ron, Phys. Rev. B25 (1982) 6496-6499.
[67] Mössbauer Isomer Shifts, edited by G.K. Shenoy and F.E. Wagner (North-Holland, Amsterdam, 1978).
[68] R.V. Pound, G.B. Benedeck, R. Drever, Phys. Rev. Lett. 7 (1961) 405-408.
[69] R. Ingalls, Phys. Rev. 155 (1967) 157-165.
[70] D.N. Pipkorn, C.K. Edge, P. Debrunner, G. De Pasquali, H.G. Drickamer, H. Frauenfelder, Phys. Rev. 135 (1964) A1604-A1612.
[71] D. Larcher , D. Bonnin , R. Cortes , I. Rivals , L. Personnaz , J. M. Tarascon , J. Electrochem. Soc. 150 (2003) A1643-A1650.
[72] S. Laruelle , S. Grugeon , P. Poizot , M. Dolle , L. Dupont , J. M. Tarascon , J. Electrochem. Soc. 149 (2002) A627-A634.
[73] P. Poizot , S. Laruelle , S. Grugeon , L. Dupont , B. Beaudoin , J. M. Tarascon , C. R. Acad. Sci., Ser. IIc: Chim. 3 (2000) 681-691.
[74] P. Poizot, S. Laruelle, S. Grugeon, L. Dupont, J.-M. Tarascon, Nature 407 (2000) 496-499.
[75] X.H. Huang, J.P. Tu, C.Q. Zhang, F. Zhou, Electrochimica Acta 55 (2010) 8981-8985.